INTERNATIONAL JOURNAL OF GEOMAGNETISM AND AERONOMY
VOL. 5, GI2002, doi:10.1029/2004GI000064, 2004

Simulation of generation and propagation of acoustic gravity waves in the atmosphere during a rocket flight

R. R. Ahmadov, and V. E. Kunitsyn

Faculty of Physics, Moscow State University, Moscow, Russia

Received 17 February 2004; accepted 18 June 2004; published 22 October 2004.

[1] A model is created for the simulation of generation and propagation to large horizontal distances of the atmosphere waves generated by supersonic rocket flight. For this purpose, the system of two-dimensional nonlinear equations of the geophysical fluid dynamics was solved by the numerical method. It was found that a rocket flight excites a wide spectrum of waves in the atmosphere: from high-frequency acoustic waves to low-frequency internal gravity waves propagating to thousands kilometers without considerable attenuation. We simulated the ionospheric disturbances generated by propagation of these waves, taking into account the geomagnetic field influence. The analysis of our results and their comparison to the experimental data show that our model makes it possible to predict more correctly and in detail the properties of the atmospheric and ionospheric disturbances generated by rocket launchings. *INDEX TERMS:* 0341 Atmospheric Composition and Structure: Middle atmosphere–constituent transport and chemistry; 0350 Atmospheric Composition and Structure: Pressure, density, and temperature; 3337 Meteorology and Atmospheric Dynamics: Numerical modeling and data assimilation; *KEYWORDS:* Acoustic gravity waves (AGW); Generation of AGW; Rocket launchings.

Citation: Ahmadov, R. R., and V. E. Kunitsyn (2004), Simulation of generation and propagation of acoustic gravity waves in the atmosphere during a rocket flight, *Int. J. Geomagn. Aeron., 5,* GI2002, doi:10.1029/2004GI000064.

1. Introduction

[2] A rocket flight with working engine causes some powerful disturbances in the ionosphere. A disturbance in the ionosphere at a large distance from the launch location and flight trajectory was for the first time detected in 1959 during the launching of the Vanguard 2 satellite [*Karlov et al.*, 1980]. During more than 40 years since that time, the observations of the upper atmosphere state using various radiophysical methods were intensively conducted in the world during carrier rocket (CR) launchings. The study of the ionosphere response to rocket launchings is of a great importance for the atmosphere science, because it would make it possible to study in detail various physical processes occurring in the upper atmosphere. The Earth atmosphere is an unique laboratory for studies of many physical processes, such as variation in photochemical reactions, propagation of shock waves (SW), formation of unstable structures in the ionosphere plasma, generation and propagation of large-scale atmosphere waves, etc. The important feature of rockets, as a source of a disturbance, is that they are located directly in the ionosphere F region.

[3] Analyzing the results of numerous experimental works performed in different time using various observation methods [*Adushkin et al.*, 2000; *Karlov et al.*, 1980], one can state that disturbances in the upper atmosphere are observed in all cases of CR launching. These disturbances are mainly of two types: the first and second types are the generation of long-living large-scale irregularities in the ionosphere and generation of wave-like attenuating oscillations in the upper atmosphere propagating to large distances from the source, respectively. The cause of the generation of the first type is the development of the Rayleigh-Taylor and Perkins instabilities in the plasma [*Adushkin et al.*, 2000] and distortion of the ionosphere photochemistry caused by the release of the combustion products of the rocket propulsion system [*Karlov et al.*, 1980], etc. The second response arises due to the propagation of SW in the atmosphere with the following generation of acoustic gravity waves (AGW). A typical feature of this type of disturbance is that AGW are observed at large distances (about 1000 km) from the rocket trajectory.

[4] According to the observation data [*Adushkin et al.*, 2000], during rocket launchings a few wave packets are detected in the ionosphere. SW are registered the first out

1524–4423/04/2004GI000064$18.00

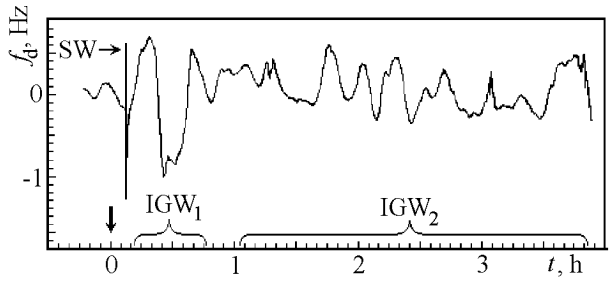

Figure 1. Dependence on time of the frequency Doppler shift during the launching of the Soyuz CR. Time is counted from the start moment.

of them. The type of rocket, the orientation of the orbit plane relative to the rocket motion plane, and the length of the oblique short-wave radio path influence weakly the studied parameters of SW. The main input is provided by the diurnal seasonal behavior. No responses to signal of oblique short-wave sounding similar to the response to SW were detected in the natural conditions. It is due to the fact that in the ionosphere plasma there are absent disturbances with timescales of 1–4 min with the form similar to the profile typical for SW. Weak wave disturbances belonging to the low-frequency acoustic range (LFA_1) are observed after SW propagation. The second group of waves (LFA_2) in the signal response appears in a few tens of minutes after the start. Also the arrival of one more group of waves (LFA_3) is possible on the background of LFA_2. The periods of these acoustic disturbances vary in the range 2.9–5.3 min. Internal gravity waves (IGW) are also inherent part of wave disturbances accompanying rocket launching. According to the data available the period range of IGW observed in the disturbances spectrum splits into three bands: up to 10 min, 15–30 min, and 75–100 min. The first packet (IGW1) appears in the signal spectrum after the intersection of the CR plane by the reference radio path and SW passage. This wave packet was detected not only in the direct vicinity of the active part of rocket motion trajectory but also at distances of about 1000 km and more. The second wave packet (IGW2) appears in a few tens of minutes after the first one and can be registered during a few hours. At remote distances of about 1000 km and more, the front of the disturbances is almost vertical with a small advance in time relative to the disturbance appearance at higher altitudes.

[5] IGW with periods of 15–75 min were registered over the Arecibo observatory (at a distance of >1000 km from the source) by the incoherent scatter radar after the launching of the space shuttle CR from the Kennedy Space Center (KSC) site on 27 June 1982 [*Noble*, 1990]. Similar results were obtained at the launching of the Soyuz CR from Baikonur site on 12 December 1990. Figure 1 shows the variations in the Doppler frequency registered during this launching at the Tashkent–Tomsk circuit crossing the active part of the rocket motion trajectory [*Adushkin et al.*, 2000].

[6] The above mentioned disturbance properties are also confirmed by other researchers. Acoustic waves (AW) with period about 1.5–4 min were revealed during launchings time of spacecrafts Apollo 12 and Apollo 13 using the Doppler sounding of the ionosphere at frequencies of 4824 and 6030 kHz and microbarographs net [*Karlov et al.*, 1980]. The experimental data obtained give values of the phase and group velocities of the wave equal to 700–800 and 220–450 m s^{-1}, respectively.

[7] Observations were also carried out using high-frequency and Doppler sounding during launchings of the space shuttle on 28 February 1990 and 28 April 1991 [*Jacobson and Carlos*, 1994]. The ionosphere wave-like disturbances with periods of 150–250 s were detected in all cases. Calculations show that the N form pulse observed in the ionosphere due to shuttle flight propagates in the upper atmosphere with the speed of sound. Disturbances with a few cycles with a period of about 200 s are observed 700–800 s after that. Other authors also registered SW caused by launchings of space shuttle which propagate in the Earth atmosphere with a horizontal velocity of 600–700 m s^{-1}. SW with a phase velocity of 700–800 m s^{-1} was also detected during the launching of the Apollo CR.

[8] A new activity in studies of ionosphere disturbances caused by sources of various types including rocket launchings began with development of the Global Positioning System (GPS) in the 1990s. High density of the GPS receivers net and sufficient regularity of rocket launchings from various rocket sites make it possible to study this phenomenon within wide time and spatial scales. *Calais and Minster* [1998] presented a detailed analysis of the observation results obtained by GPS receivers during the launching of the space shuttle Columbia CR on 18 October 1993. The authors registered two wave packets of oscillations of the total electron content (TEC). The first wave packet is a N form pulse with a period of about 300 s. It does not show any wave dispersion, whereas the second wave packet demonstrates obviously the dispersion and consists of several cycles. The calculations show that the horizontal phase velocity of the first wave propagation is of about 800 m s^{-1} at higher altitudes. In 15 min after the passing of the first packet the second wave packet propagating with a horizontal velocity of about 300 m s^{-1} is observed. Wave disturbances of TEC during launchings of Soyuz and Proton CR from the Baikonur site were detected using the GPS system [*Afraimovich et al.*, 2001]. On the basis of these results one can state that the ionosphere response during the considered launchings has a shape of N wave. The disturbances amplitude varies from 0.03 TECU to 0.9 TECU (total electron content units is commonly used unit of TEC, 1 TECU is equal to 10^{16} m^{-2}). The period of these waves varies from 132 to 288 s.

[9] In a few papers attempts have been undertaken to explain from the theoretical point of view the observed disturbances in the ionosphere during a rocket flight. The analytic and numerical calculations predict correctly the arrival time of the first ionosphere waves pulse from such sources. However, no model can still explain the cause of the appearance of the second wave packet following the first pulse [*Calais and Minster*, 1998].

[10] *Arendt* [1971] assumes that the shock wave formed at rocket flight splits at a height of about 160 km in the ionosphere to ion acoustic and normal acoustic modes. The

facts that the motion velocity of the first disturbance found during the launchings of Apollo 14 and Apollo 15 is close to the velocity of the ion acoustic mode and that the second disturbance velocity is close to the velocity of the normal acoustic wave are considered by *Arendt* [1971] to be in favor of the proposed hypothesis.

[11] Some authors interpret the appearance of the secondary waves as a consequence of the reflection from the solid Earth surface. However, the same disturbances are observed during earthquakes and ground explosions, and in this case the waves can not be explained by a reflection [*Calais and Minster*, 1998].

[12] *Calais and Minster* [1998], *Nagorsky* [1998] and *Tolstoy et al.* [1970] assume that the second wave packet is a result of the capture of AGW in the atmospheric mesosphere–thermosphere waveguide (MTW), which is located between the mesopause (about 100 km) and the thermocline (about 120 km). Nevertheless, these assumptions are not proved by conclusions of theoretical works. None of the existing models can correctly predict the generation of long-period IGW from short-lived disturbances pulses. Moreover, on the basis of the existing models, it is impossible to describe completely the total picture of ionosphere disturbances.

[13] The above mentioned facts clearly show that the great experimental material dedicated to the atmosphere and ionosphere disturbances generated at rocket launchings has been accumulated. However, the interpretation of the space-time characteristics of these disturbances is obviously insufficient. The goal of our paper is to simulate the ionosphere wave-like disturbances caused by rocket launchings using contemporary achievements in the field of numerical simulation of geophysical fluid dynamics problems and also to perform a preliminary comparison of the obtained results to experimental data.

2. The Model

2.1. Fluid Dynamics Equations

[14] We are interested in the wave-like disturbances of the ionosphere electron density observed at large distances from the rocket flight trajectory. These waves (AGW) may be observed from other types of disturbance sources such as explosions, earthquakes, meteors etc. We should simulate generation and propagation of these waves in the lower atmosphere and the ionosphere.

[15] IGW are the most intense part of the AGW spectrum. Since the 1960s very many papers were dedicated to study of the atmosphere IGW properties. In these papers a solution of the fluid dynamics equations by analytical or numerical methods is one of the widely used methods [*Francis*, 1975]. New direction in physics of the atmosphere waves was born in the recent years due to the increase of computer processing rate and computational fluid dynamics development. This direction is the study of IGW propagation using numerical solution of the nonlinear geophysical fluid dynamics equations [*Zhang and Yi*, 2002]. Application of such numerical methods makes it possible to solve numerous problems such as simulation of the intense atmosphere waves excitation at strong impacts of supersonic rocket flights on the environment etc. Thus in order to solve the direct problem, i.e., simulation of an atmosphere disturbance, we have to solve the fluid dynamics equations system with corresponding initial and boundary conditions. Strong inhomogeneous medium exists in the atmosphere around the rocket, being formed by the release of exhausts out of the rocket engine and by the supersonic rocket flight. Therefore it is very complicated and inconvenient to solve the atmosphere disturbances problem during rocket flight in a general form. So the atmosphere region simulated by us is located at some distance from the rocket trajectory, that is, there where the strong SW generated by the rocket flight is attenuated and is transformed into an intense acoustic pulse. Further, there is a nonlinear stretching of this pulse and generation of the AGW wide spectrum with the following disturbance of the ionosphere plasma as result of collision to neutral particles etc. Acoustic pulse is introduced into our model by determination of corresponding boundary conditions. We will come back to the parameters of this pulse in the next paragraph.

[16] The propagation of AGW in the atmosphere is described by the solution of the fluid dynamics equations system:

$$\frac{\partial \rho}{\partial t} + \nabla(\rho \mathbf{v}) = 0$$

$$\rho\left(\frac{\partial \mathbf{v}}{\partial t} + (\mathbf{v}, \nabla)\mathbf{v}\right) = -\nabla p + \rho \mathbf{g} + \mathbf{F}^d \tag{1}$$

$$\rho\left(\frac{\partial (c_v T)}{\partial t} + (\mathbf{v}, \nabla)(c_v T)\right) = -p(\nabla, \mathbf{v}) + Q^d$$

$$p = \frac{\rho}{m_0} RT$$

The first, second, third, and fourth equations are continuity equation, momentum conservation equation, energy conservation equation, and equation of the ideal gas state, respectively. The Coriolis force is insignificant for such relatively rapid motions, therefore we neglect by it. Here ρ, T, p, and $\mathbf{v}$ are the density, temperature, pressure, and velocity of environment particles motion, respectively. The values of $\mathbf{g}$, $\mathbf{F}^d$, and Q^d are the gravitational acceleration, viscosity force, and the heat absorbed due to wave dissipation, respectively. The values of c_v, m_0, and R are the specific heat of gas at constant volume, relative molecular mass of air, and the universal gas constant, respectively.

[17] The viscosity force in this model is introduced as the resistance force in the Rayleigh form $\mathbf{F}^d = -\alpha \mathbf{v}$ [*Sedunov*, 1991]. This form of a simple parameterization of the viscous friction forces is often used in complex fluid dynamics calculations. The kinematics friction coefficient $\chi = \alpha/\rho$ increasing with height was chosen after the testing of the model at various values. The heat conductivity play the main role at the energy attenuation of such large wave motions [*Zhang and Yi*, 2002], that is, the dissipative part in

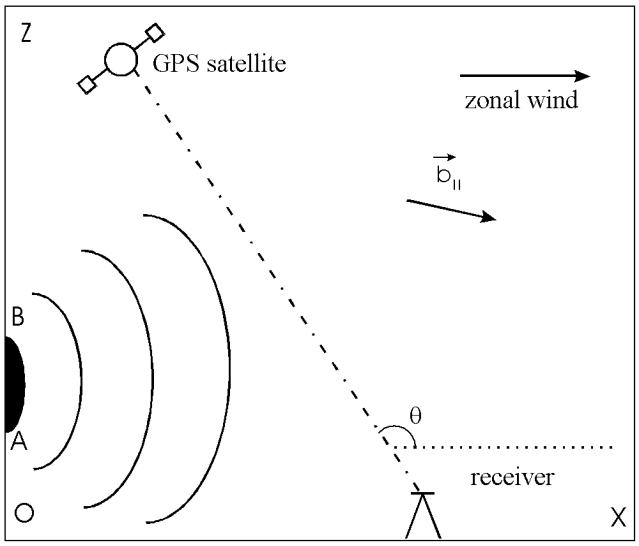

Figure 2. Coordinate system and schematic diagram presenting the wave propagation from the source and the ionosphere observation using GPS system.

the temperature equation is equal to $Q^d = k\Delta T$, where k is the coefficient of air heat conductivity.

[18] Each thermodynamic parameter in equations system (1) is split to two parts: the stationary part denoted by index 0 and the disturbed one denoted by a dash:

$$\rho = \rho_0 + \rho' \qquad T = T_0 + T'$$

$$p = p_0 + p' \qquad v_x = u + U_0$$

where U_0 is the horizontal velocity of the background zonal wind in OX direction (the meridional wind is not taken into account). Assuming a hydrostatic equilibrium for the background atmosphere, for the two-dimensional, plane-parallel, compressible atmosphere we obtain after some transformations a system consisting of equations in partial derivatives and the equation of the ideal gas state.

$$\frac{\partial \rho'}{\partial t} = -\frac{\partial}{\partial x}[(\rho_0 + \rho')u] - \frac{\partial}{\partial z}[(\rho_0 + \rho')w] - U_0\frac{\partial \rho'}{\partial x}$$

$$\frac{\partial u}{\partial t} = -u\frac{\partial u}{\partial x} - U_0\frac{\partial u}{\partial x} - w\frac{\partial u}{\partial z} - w\frac{\partial U_0}{\partial z}$$

$$-A_1\frac{1}{\rho_0 + \rho'}\frac{\partial p'}{\partial x} - A_2\chi u$$

$$\frac{\partial w}{\partial t} = -u\frac{\partial w}{\partial x} - U_0\frac{\partial w}{\partial x} - w\frac{\partial w}{\partial z}$$

$$-A_1\frac{1}{\rho_0 + \rho'}\frac{\partial p'}{\partial z} - A_3\frac{\rho'}{\rho_0 + \rho'} - A_2\chi w \qquad (2)$$

$$\frac{\partial T'}{\partial t} = -u\frac{\partial T'}{\partial x} - U_0\frac{\partial T'}{\partial x} - w\frac{\partial (T_0 + T')}{\partial z}$$

$$-A_4\left(\frac{\partial u}{\partial x} + \frac{\partial w}{\partial z}\right) + A_5\left(\frac{\partial^2 T'}{\partial x^2} + \frac{\partial^2 (T_0 + T')}{\partial z^2}\right)$$

$$p' = \frac{\rho_0 T' + \rho' T_0 + \rho' T'}{m_0}$$

Here u and w are the horizontal and vertical components of atmosphere particles motion velocity in wave, respectively, and A_{1-5} are constants. The frame of reference used here is shown in Figure 2, where the OZ axis is directed vertically upward, and the OX axis is horizontal and lies on the Earth surface.

2.2. Shock Waves

[19] In order to introduce into our model the boundary conditions describing the disturbance source, one should know the exact parameters of SW generated by the rocket flights. Launching of CR of the space shuttle type is considered for determination of the Mach cone location and orientation in the atmosphere generated by the rocket flight. All launchings of the space shuttle CR have the following stages of flight in the Earth atmosphere. The launching of CR, its ascent to some altitude where the stages are separated and the main engine burns and works during about 7 min [*Jacobson and Carlos*, 1994]. Only during this stage of the flight (called "the main engine burn" (MEB)), the shuttle and its external tank of liquid fuel continue ascending up to 105–110 km and then accelerate in the horizontal flight. The horizontal flight of MEB extends from 300 km up to 1400 km from the launching point. During the horizontal flight the shuttle velocity increases from 2.5 km h^{-1} to 7.5 km h^{-1} (up to the end of MEB). Thus the horizontal flight is a supersonic one and whichever waves are generated (acoustic or internal gravity ones), they have to propagate perpendicularly to the flight trajectory. Moreover many other observations show that the generation of AGW occurs mainly during the horizontal rocket flight [*Afraimovich et al.*, 2001].

[20] Taking the above into account, we introduce the disturbance source into the simulation model in the following manner. Let the vertical coordinate plane XOZ (see Figure 2) be perpendicular to the trajectory of the horizontal rocket flight. One can assumed that a single strong nonlinear acoustic pulse which is further transformed into an AGW packet enters into the computed domain from the left-hand boundary (region AB in Figure 2). To take parameters of this pulse, we consider the general properties of SW from rockets. At the supersonic streamline of the rocket at large distances from it the disturbances caused by SW are weak and therefore may be considered as a cylindrical sound wave divergent from the axis passing through the rocket and parallel to the direction of the streamline [*Landau and Lifshits*, 1988]. Two shock waves are formed in the

cylindrical sound pulse. The velocity in the front break increases by a jump from zero, then there follows the region of a gradual compression decrease changed by a rarefaction, and after that pressure again increases by a jump in the second break. However, the cylindrical sound pulse is specific (as compared with both flat and spherical cases) and can have no rear front: the tendency of the particles motion velocity to zero occurs only asymptotically. From here one can conclude that the cylindrical sound pulse emitted by a rocket flight have a complicated asymmetric form. However, in the first approximation one may take this wave in a sinusoidal form. As it has been noted in section 1, this is also proved by the fact that the initial acoustic wave at large distances is so leveled that its form influences weakly the response form. Running ahead, one may say that the results of our calculations also confirm this fact. As the diameter of the cylindrical pulse is small as compared to the vertical size of the considered region (XOZ), we accepted the front of the wave passing through the region boundary as flat. The acoustic pulse is introduced into the model in such a form that the expression for the horizontal component of the oscillation velocity of air particles on the OZ axis would be

$$u = u_m \sin\left(\frac{2\pi(t-t_0)}{P}\right)$$

$$\times \exp\left[-\left(\frac{z-z_m}{D_z}\right)^2\right] \quad t_0 \le t \le t_0 + P \tag{3}$$

where u_m, t_0, P, z_m, and D_z are the amplitude, the moment of the pulse arrival, period, altitude of the axis of the sound cylinder from the Earth surface, and the Gauss scale characterizing the cylinder transverse dimension, respectively.

[21] The values of the density and pressure in the wave can be calculated using formulae describing simple nonlinear acoustic waves [*Rudenko and Soluyan*, 1975]:

$$\rho = \rho_0\left(1 + \frac{\gamma-1}{2}\frac{u}{c}\right)^{2/(\gamma-1)}$$

$$p = p_0\left(1 + \frac{\gamma-1}{2}\frac{u}{c}\right)^{2\gamma/(\gamma-1)} \tag{4}$$

where γ is the adiabatic constant, c is the speed of sound. The value of the temperature perturbation may be determined from the state equation. After that one can easily introduce the boundary conditions into equation (2) for all values at the OZ left-hand side boundary of the simulation region. These boundary conditions provide a transmission of the disturbance from the medium around the rocket trajectory to the atmosphere region considered by us. As for the simulation of the second atmosphere region located to the left from the rocket trajectory, in this case the same boundary conditions will be at the right-hand boundary of the computation domain.

2.3. Ionosphere Disturbances

[22] Solving equations system (2) one can found the spatial and time distribution of all parameters looked for in the calculation region. As the final goal of our work is a comparison of the simulation results with the data of observations, disturbances in the electron concentration in the ionosphere should be calculated. For this purpose we consider the continuity equation for charged particles:

$$\frac{\partial N_e}{\partial t} + \nabla(N_e \mathbf{v}_e) = P_e - L_e \tag{5}$$

Here N_e is the concentration of electrons in undisturbed ionosphere, $\mathbf{v}_e$ is the motion velocity of free electrons in the ionosphere, and P_e and L_e are the production and loss rates due to chemical processes, respectively. *Andreeva et al.* [2001] showed that due to collisions with neutral particles during AGW propagation the ionosphere plasma obtains the velocity (this is most correct for the F layer):

$$v_e \approx (\mathbf{v}, \mathbf{b})\mathbf{b} \tag{6}$$

where $\mathbf{b} = \mathbf{B}/|\mathbf{B}|$ is a unit vector along the Earth magnetic field (see Figure 2). We assume that the magnetic field is homogeneous in the simulation domain. Taking into account equation (6) and neglecting formation and loss of charged particles, after integration of (5) we obtain

$$\Delta N_e(x,z,t) = -\frac{dN_e}{dz}\int_{t_0}^{t}(b_x b_z u + b_z^2 w)d\tau$$

$$-N_e\int_{t_0}^{t}\left[b_x^2\frac{\partial u}{\partial x} + b_x b_z\left(\frac{\partial u}{\partial z} + \frac{\partial w}{\partial x}\right) + b_z^2\frac{\partial w}{\partial z}\right]d\tau \tag{7}$$

where b_x and b_z are the components of a unit vector of the Earth magnetic field. Here the first integral characterizes the variation in the concentration due to the motion of some volume of the ionosphere and the second integral is a consequence of the processes of compression or rarefaction in the plasma. Using this formula one can calculate the variations in the electron concentration in the ionosphere at AGW propagation at this point in the given moment of time. In our calculations we took the profile (see Figure 3) consisting of two layers as the background ionosphere electron concentration. We used the IGRF model (http://nssdc.gsfc.nasa.gov/space/model/models/igrf.html) for determination of the geomagnetic field components. If one neglects the magnetic field influence, that is everywhere $\mathbf{b}\|\mathbf{v}$, then

$$\Delta N_e(x,z,t) = -\frac{dN_e}{dz}\int_{t_0}^{t} w d\tau - N_e\int_{t_0}^{t}\left(\frac{\partial u}{\partial x} + \frac{\partial w}{\partial z}\right)d\tau \tag{8}$$

As noted in section 1, the determination of TEC variation (ΔTEC) in the ionosphere in various directions, i.e., between the receiver and GPS satellite (see Figure 2), is of a great importance for observations of the ionosphere state:

$$\Delta\mathrm{TEC} = \int_{\text{receiver}}^{\text{satellite}} \Delta N_e dr$$

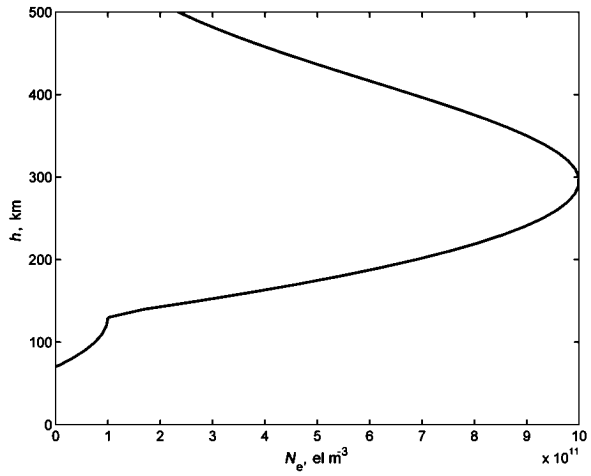

Figure 3. Vertical profile of the electron concentration in the background ionosphere.

Integrating, we assume that above the simulation domain $\Delta N_e \approx 0$. It should be noted that the real ionosphere is horizontally inhomogeneous but we confine our consideration by a parallel-sided ionosphere.

3. Numerical Method

[23] There are many numerical methods for solution of fluid dynamics equations. For a numerical solution of equation system (2) one have to choose an optimal approximation method suitable for this problem. Problem solutions of computing geophysical fluid dynamics are very complicated by the fact that here writing the algorithm one has to take into account the boundary conditions, abilities of computers (rate and random access memory), calculation methods, etc. Generally the problem depends on many parameters and one has to choose and adapt a numerical method for the only particular problem.

[24] The processes considered in this problem are nonstationary. Since the disturbances are very quick variable the approximated equations should be integrated with a small time step. The wave propagation time at large distances is tens of minutes and so thousands of iterations are required. Taking into account this fact and the nonlinearity of the equation system, one can conclude that in this case the explicit finite difference method of integration of fluid dynamics equations is the most suitable. It is known that the background atmosphere density ρ_0 decreases very sharply with height and large gradients can lead to nonphysical oscillations in the numerical solution. This fact should be taken into account choosing a numerical method [*Oran and Boris*, 1987]. Taking into account this fact, after testing of various difference methods we created a numerical method, using the some properties of the LCPFCT algorithm [*Oran and Boris*, 1987]. During the recent 10–15 years this method has been successfully used for solution of various types of fluid dynamics problems.

[25] At first for numerical solution of equation (2), one has to construct a uniform orthogonal difference grid in which the physical boundaries are located along the grid lines. The difference grid is chosen in such a way that its lower boundary coincides with the rigid flat Earth surface along the OX axis (see Figure 2). For example, the value of ρ_{ik}^{tn} is the value of the density perturbation in the cell center with coordinates x_i and z_k at the time moment t^n. Indices i and k denote the number of the calculation cell (i along the horizontal, $i = 1, ..., I$, and k along the vertical, $k = 1, ..., K$) and n is the number of the time layer ($n = 0, 1, ..., N$). Choosing parameters of the difference grid, the Courant-Friedrichs-Lewi conditions should be fulfilled [*Durran*, 1999], that is for the stability of the solution of equations system (2) the following condition $\Delta t[c+\sqrt{u^2+w^2}/\min(\Delta x, \Delta z)] < 1$ should be fulfilled. Here Δt, Δx, and Δz are the sizes of the grid steps in time and in the horizontal and vertical directions, respectively. The following parameters of the difference grid were chosen: the steps in altitude, horizontal coordinate, and time are 5 km, 10 km, and 0.5 s, respectively. The height and width of the grid are 400 km and 2000 km, respectively.

[26] We split the system (2) to two systems, where the first equation system contain in the right-hand side only the vertical components and the second one contains only the components along the horizontal direction:

$$\frac{\partial \rho'}{\partial t} = -\frac{\partial}{\partial z}[(\rho_0 + \rho')w]$$

$$\frac{\partial u}{\partial t} = -w\frac{\partial u}{\partial z} - w\frac{\partial U_0}{\partial z}$$

$$\frac{\partial w}{\partial t} = -w\frac{\partial w}{\partial z} - A_1\frac{1}{\rho_0+\rho'}\frac{\partial p'}{\partial z} - A_3\frac{\rho'}{\rho_0+\rho'} - A_2\chi w \quad (9)$$

$$\frac{\partial T'}{\partial t} = -w\frac{\partial (T_0+T')}{\partial z} - A_4\frac{\partial w}{\partial z} + A_5\frac{\partial^2 (T_0+T')}{\partial z^2}$$

$$p' = \frac{\rho_0 T' + \rho' T_0 + \rho' T'}{m_0}$$

$$\frac{\partial \rho'}{\partial t} = -\frac{\partial}{\partial z}[(\rho_0 + \rho')u] - U_0\frac{\rho'}{\partial x}$$

$$\frac{\partial u}{\partial t} = -u\frac{\partial u}{\partial x} - U_0\frac{\partial u}{\partial x} - A_1\frac{1}{\rho_0+\rho'}\frac{\partial p'}{\partial x} - A_2\chi u$$

$$\frac{\partial w}{\partial t} = -u\frac{\partial w}{\partial x} - U_0\frac{\partial w}{\partial x} \quad (10)$$

$$\frac{\partial T'}{\partial t} = -u\frac{\partial T'}{\partial x} - U_0\frac{\partial T'}{\partial x} - A_4\frac{\partial u}{\partial x} + A_5\frac{\partial^2 T'}{\partial x^2}$$

$$p' = \frac{\rho_0 T' + \rho' T_0 + \rho' T'}{m_0}$$

This method increases accuracy of the numerical scheme in respect of time. The obtained systems of one-dimensional equations are separately solved using the one-dimensional module developed for equations system solution in the time interval from t to Δt. Numerical integration of the equations is performed in the horizontal and vertical directions alternately. Each couple of sequential integrations is an advancement of the solution by one complete step in time. The application of the numerical method for the continuity equation in (9) gives

$$\overline{\rho_{ik}^{tn}} = \rho_{ik}^{tn} - \frac{\Delta t}{4\Delta z}[(\rho_{ik}^{tn} + \rho_{ik+1}^{tn})(w_{ik}^{n} + w_{ik+1}^{n})$$

$$-(\rho_{ik}^{tn} + \rho_{ik-1}^{tn})(w_{ik}^{n} + w_{ik-1}^{n})]$$

Here $\overline{\rho_{ik}^{tn}}$ denotes an intermediate value of the disturbance in the density. A diffusion part, which provides the stability, should be included in this equation:

$$\tilde{\rho}_{ik}^{tn} = \overline{\rho_{ik}^{tn}} + \nu(\rho_{ik+1}^{tn} - 2\rho_{ik}^{tn} + \rho_{ik-1}^{tn})$$

where $\tilde{\rho}_{ik}^{tn}$ is also an intermediate value of the disturbance in the density, ν is the dimensionless diffusion coefficient. At the next stage this large numerical diffusion is minimized using an adding of antidiffusion fluxes. The final value of the density disturbance in the new time moment $n+1$ is

$$\rho_{ik}^{tn+1} = \tilde{\rho}_{ik}^{tn} - f_{k+1/2}^{ad} + f_{k-1/2}^{ad}$$

where $f_{k+1/2}^{ad} = \mu(\overline{\rho_{ik+1}^{tn}} - \overline{\rho_{ik}^{tn}})$ is the antidiffusion flux, μ is the dimensionless coefficient of the antidiffusion. The values of the velocities and temperature disturbances are found by the same method.

[27] Unlike in the fluxes correction method LCPFCT, we did not use the special limitation applied to the antidiffusion fluxes for conservation of a positivity of solution, because the variables in (2) can be positive and negative values. Thus we get rid of such problems as fluxes synchronization [*Oran and Boris*, 1987] etc. That is why we wrote the equation system (2) in terms of variations in density and temperature, but not of their absolute values.

[28] For the sake of stability the nonlinear components in (9) are approximated in the following manner [*Durran*, 1999]:

$$w\frac{\partial w}{\partial z} = \frac{1}{2}(w_{ik+1}^{n} + w_{ik-1}^{n})\left(\frac{w_{ik+1}^{n} - w_{ik-1}^{n}}{2\Delta z}\right)$$

Equations system (10), where the components related to the horizontal direction are present in the right-hand side, is solved by the same method.

[29] Solving equations systems (2) one has to assign initial and boundary conditions. The initial conditions for velocity, density disturbances, and temperature were chosen to be zero. Four walls exist in this model. There are two horizontal and two vertical walls, for which the boundary conditions should be assigned. Points at the boundaries may be considered as inner due to introduction of fictitious cells. The values within these sells are assigned by the boundary conditions. The same boundary conditions as in the case of tangential breaks are applied at the lower boundary [*Landau and Lifshits*, 1988] that is the variables undertake no jump passing through the Earth surface. At the upper and right-hand side boundaries we applied usual boundary conditions for provision of waves passage through these walls without any considerable reflection [*Durran*, 1999]. At the left-hand side boundary we used the boundary conditions in form (3), which provide penetration of disturbances into the calculations region. After the pulse passage through the boundaries the same boundary conditions are applied there as for the right-hand side boundary.

4. Simulation

4.1. The Calculation Results

[30] Thus equations system (2) with the initial and boundary conditions was solved, using the computer program MADRL created by us. The profiles of the background density and temperature of the atmosphere from the MSISE 90 model (ftp://nssdcftp.gsfc.nasa.gov/models/atmospheric/hwm93) were used in the simulation. We used various versions of the input data as parameters of the disturbance source. Here we present the results calculated for one case. Choosing the values of these parameters we took into account the fact that in practice it is not simple to determine precise values of the disturbances pulse parameters and they depend on the particular launching. However, as far as our main goal is to study general properties of the disturbances from such sources, we took approximate values of the parameters of the acoustic pulse: $u_m = 200$ m s^{-1}, $P = 23$ s, $z_m = 110$ km, $D_z = 10$ km [*Nagorsky*, 1998].

[31] It is widely known that the temperature stratification and the zonal wind influence the AGW propagation in the atmosphere. In order to separate these influences from each other, we considered in our calculations step-by-step different versions of the atmosphere model. At first we simulated the problem in the isothermal and quiet atmosphere where the zonal wind is absent. The results of this simulation show that after the disturbance arrival to the considered region, there are generated AW and IGW. Disturbances with scales of hundreds of kilometers are observed at considerable horizontal distances. By their spatial and time characteristics these disturbances belong mainly to the IGW class. These waves exceed considerably AW by their intensity. Figure 4 shows the part of the calculated region, where they are clearly manifested 5000 s after the passing of the disturbance through the model region boundaries. The results of the calculations show that the main component of the velocity is the horizontal one. The period of these waves varies from 6 min to 14 min and increases linearly in the process of horizontal propagation. One can see from Figure 4 that the wave fronts are almost vertical. Moreover, a

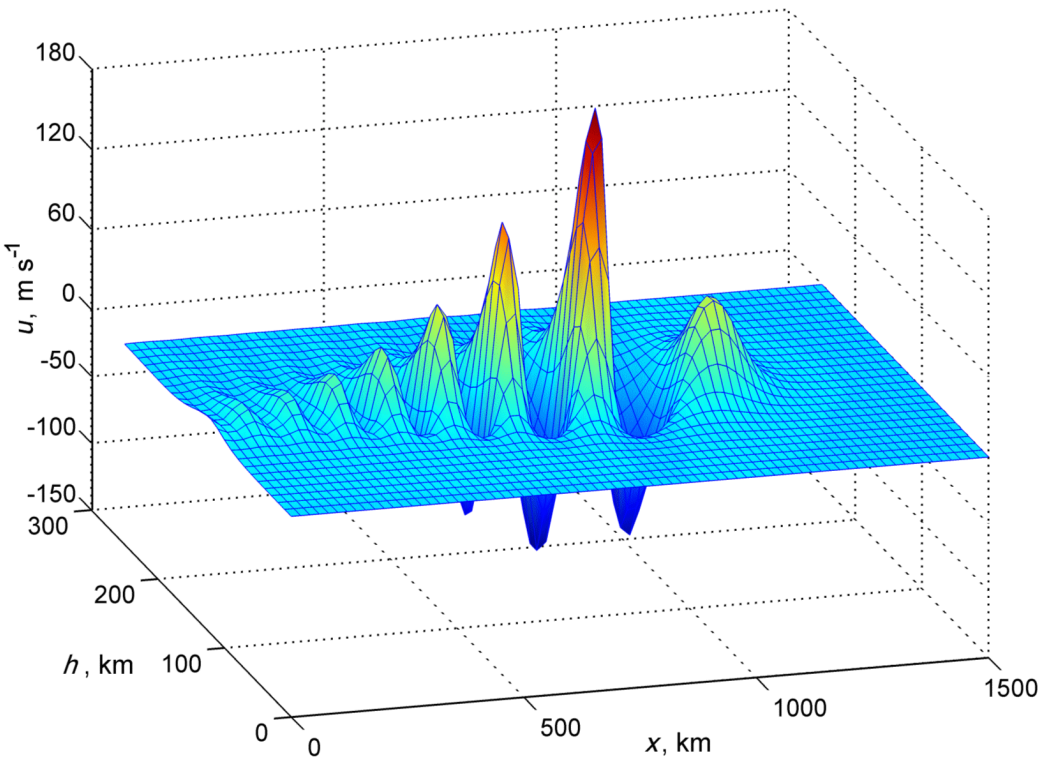

Figure 4. Horizontal component of the particle velocity versus coordinates in the isothermal atmosphere.

nonlinear deformation is observed, that is steepening of the wave profile caused by a large value of the Mach number [*Landau and Lifshits,* 1988]. It was found that disturbances in the isothermal atmosphere mainly contain a continuous spectrum of IGW. One can see in Figure 4 that the saturation point (i.e., the height of the maximum amplitude of the wave) is situated at a height of $h \approx 150$ km. All the above mentioned properties of IGW found by us agree with the results of many authors [*Francis*, 1975]. The latter results have been obtained using analytical and numerical calculations with more simple models describing the IGW propagation. This shows that our numerical method has a high enough accuracy.

[32] As it was expected, taking into account of the real profile of the atmosphere temperature leads to results quite different from the first case. Main difference is the appearance of a discrete wave spectrum which arises as a result of the ducting of the wave in the atmosphere waveguides. These waveguides are formed due to the wave reflection from the temperature gradients and the Earth surface. Many studies were performed using spectral models to investigate properties of these waves in different modes [*Francis,* 1975; *Gavrilov*, 1985]. However, our model allows us to find a common picture of AGW propagation in the real atmosphere where the picture of disturbances is formed by a superposition of all modes of the ducted waves and continuum and also by a nonlinear interaction between different harmonics. Figure 5 shows the horizontal component of the atmosphere particles velocity versus the coordinates in the time moment $t = 5000$ s for the January profiles of the atmosphere temperature and density. It is evident that the complicated shapes of wave surfaces differ considerably from the previous case. In Figure 5 ducted waves are observed at heights of 100–150 km. This wave spectrum belongs to the thermospheric modes G_0' arising as a result of the AGW ducting into MTW [*Francis*, 1975]. Comparing Figures 5 and 4, one can see that the wave amplitudes in the case of the real stratification of the temperature are much less than in the isothermal atmosphere, this fact once more proving a ducting of waves. The values of the vertical component of motion velocity of the particles in the wave, the variations in the atmosphere temperature and density demonstrate similar dependencies on time and space.

[33] Simulating the ionosphere disturbances caused by propagation of AGW, we found that characteristics of these irregularities depend strongly on the direction of the geomagnetic field. We demonstrate this fact for some cases. Figure 6 shows variation in the electron concentration versus the coordinate at the time moment $t = 5000$ s for the model with the real stratification of the density and temperature. Here Figure 6a presents the case when the magnetic field is not taken into account, that is the variation in the electron concentration is calculated using formula (8); Figure 6b corresponds to the cases when the magnetic field is directed horizontally, i.e., in the vicinity of the geomagnetic equator; Figure 6c presents the case when the magnetic field is directed vertically, i.e., in the vicinity of the magnetic pole; and Figure 6d corresponds to the situation near the

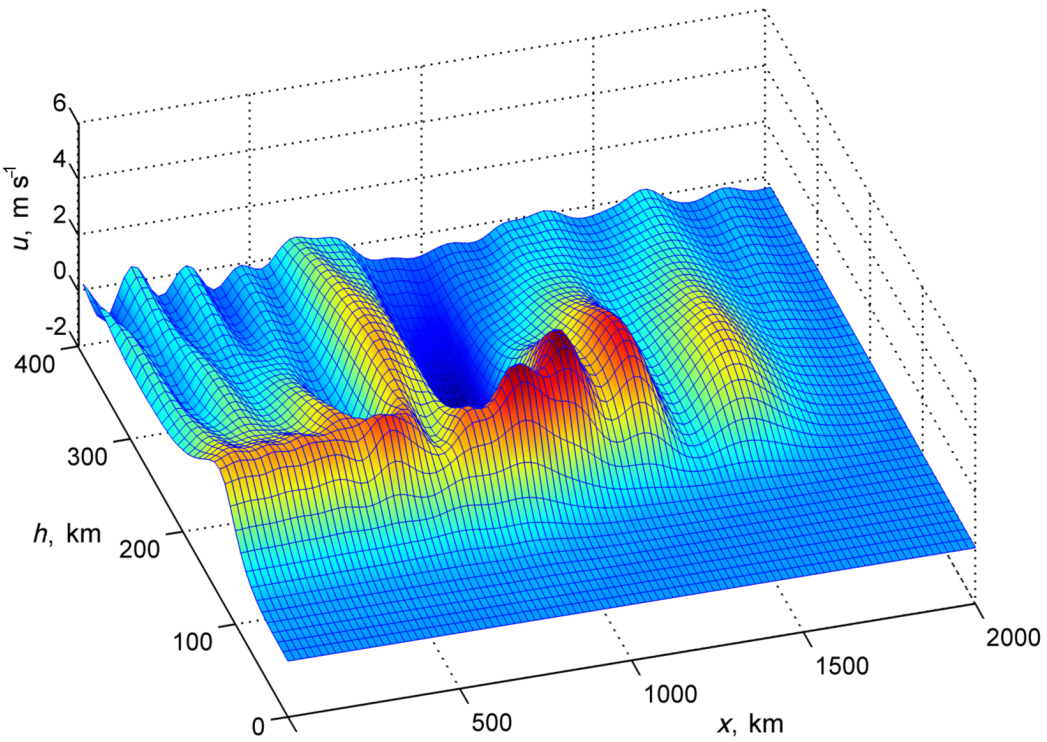

Figure 5. Horizontal component of the particle velocity versus coordinates in the atmosphere with a temperature stratification.

rocket site KSC (28.5°N, 279.3°E) (the OX axis is directed eastward). It is evident that if the magnetic field is perpendicular to the particles velocity ($b_x = 0.0$, $b_z = 0.0$), then disturbances are absent. Figure 6 demonstrates how the magnetic field changes strongly the picture of the ionosphere wave-like irregularities. Because of the vertical component the shape of the disturbances becomes oblique. Our studies show that orientation of the magnetic field influences not only the spatial picture of the ionosphere disturbances, but their time characteristics.

[34] One can see from the results that the horizontal lengths of wave-like disturbances are hundreds of kilometers, the propagation velocity is about 300 m s^{-1}, and the amplitude is of the order of a few percents of the background electron concentration. These are well-known medium-scale traveling ionosphere disturbances (TID) [*Francis*, 1975].

[35] After that we can find the disturbances in TEC along the satellite–receiver ray. We assume that this satellite is located on the XOZ plane. Figure 7 presents the variation in TEC in the vertical direction when the GPS receiver is located in the point $x = 400$ km and the elevation angle of the satellite is $\theta = 90°$ (see Figure 2). This result is for the real atmosphere and the direction of the magnetic field ($b_x = 0.51$, $b_z = -0.86$), i.e., in the vicinity of KSC. One can see from Figure 7 that the profile of the variation in TEC is rough and asymmetric. Here two wave packets are presented: the first packet is low-frequency IGWs with a period of about 20 min and the second wave packet is ducted IGWs with a shorter period. As it has been noted above, there are many modes of ducted AGW. Taking into account that all heights take part in the profile formation, one can understand the cause of the picture complicity. Moreover, the dispersion and nonlinear effects also lead to deformation of the wave profile [*Rudenko and Soluyan*, 1975]. In order to demonstrate how the picture of TEC variation changes strongly depending on the elevation angle of the satellite and the receiver location, we consider the case when the receiver is located in the point $x = 1000$ km and $\theta = 170°$. It is evident in Figure 8 that in this case quite a different picture is obtained, which differs from the previous one not only quantitatively but also qualitatively. Here AW with periods of a few hundreds seconds and also captured AW are seen.

[36] To take into account possible influence of the wind, we assume that its direction coincides with the direction of OX (see Figure 2). Inclusion of the zonal wind into model does not considerably influence the final result. It is convincingly shown in Figure 9 where three curves show the TEC variations in the same registration conditions (the receiver location $x = 600$ km and the elevation angle $\theta = 90°$) and at the same direction of the magnetic field. The first, second and third curves correspond to the January temperature profile in windless atmosphere, the January temperature profile and allowance for the zonal wind, and the July temperature profile without allowance for the wind, respectively. The more complicated structure of the secondary waves in the case of taking into account the wind can be explained by the fact that part of the waves is ducted by the wind [*Gavrilov*, 1985] and is superimposed on the other ducted waves. One can see from Figure 9 that the properties of the ionosphere response also insignificantly depend on the season. The higher am-

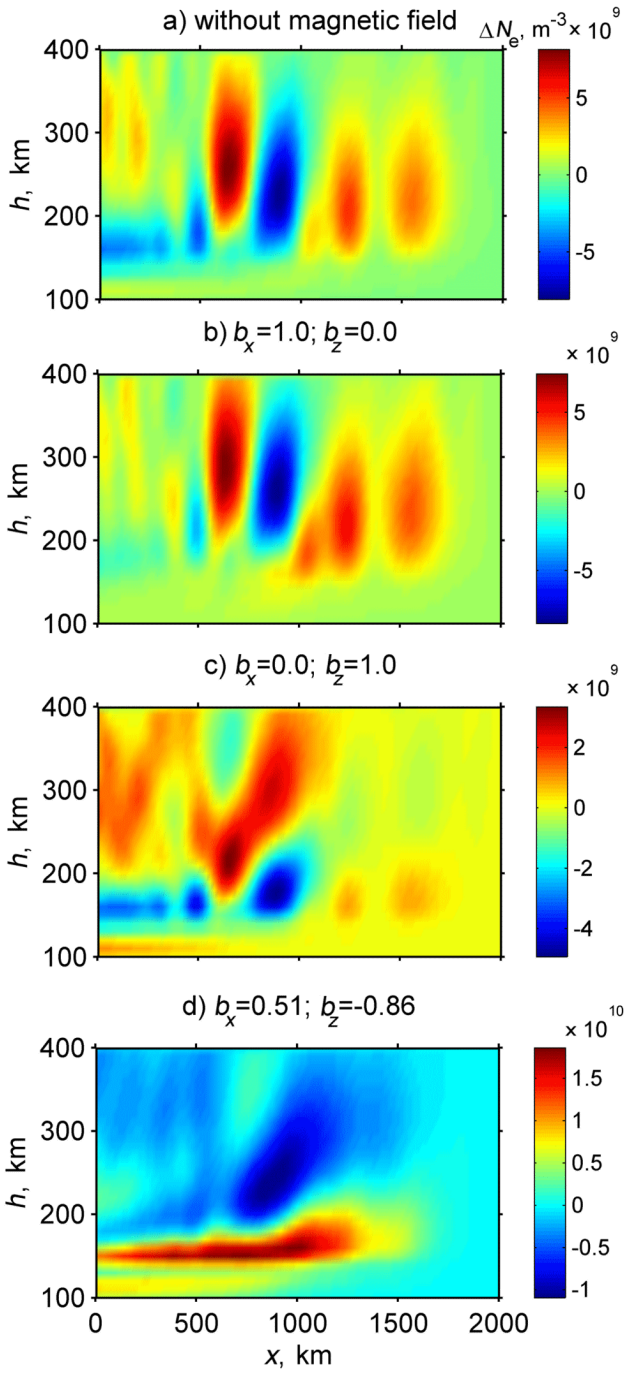

Figure 6. Spatial distribution of the electron concentration variations demonstrating the influence of the magnetic field.

plitude of the waves in July may be explained by the higher temperature of the upper atmosphere in summer than in winter. Comparing Figures 9 and 7, we see that the period of the first N form wave increases with distance, because the distances of GPS receivers from the source are different in the first and second cases. Moreover, the profile of the variation in TEC at large distances from the source becomes smoother. It can be caused by the fact that acoustic waves

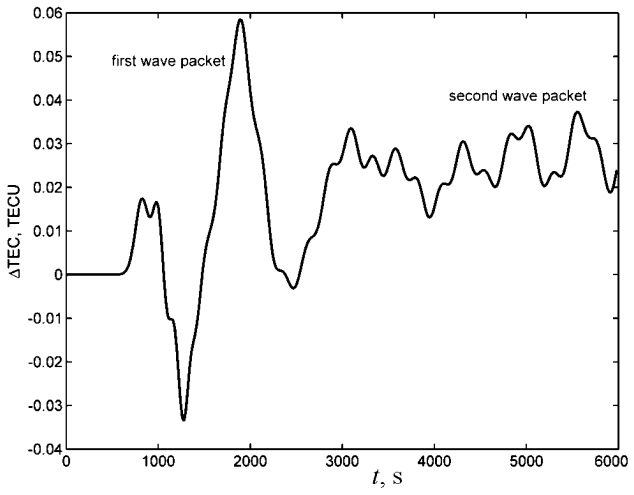

Figure 7. Time dependence of the vertical TEC disturbance.

attenuate quickly [*Francis*, 1975] and only IGW are observed at large distances from the source.

4.2. Comparison to Observations Data

[37] The preliminary comparison of the obtained results to the experimental data shows that, first our model predicts an appearance of TIDs very often observed in the atmosphere from various sources including rocket launchings. The horizontal propagation and oblique forms of TID predicted by us are observed in many experiments [*Adushkin et al.*, 2000]. If we consider the second half plane which is located to the left of the Mach cone where the angle between the magnetic field and the velocity is different, and also if we take into account variations in the magnetic field with horizontal distance, we conclude that actually the general picture of the ionosphere disturbances can have no symmetry relative the rocket trajectory. This is confirmed by the observation results carried out by the radiotomography method during the rocket launching from Plesetsk rocket site [*Kunitsyn and Tereshchenko*, 2003]. One can see from the results obtained that our numerical calculations provide the entire spectrum of the disturbances observed from rockets (acoustic waves, internal gravity waves, and secondary ducted waves). As it has been noted in section 1, all these waves are observed in the experiments conducted by different methods. The importance of our results is confirmed by the fact that our model (unlike the previous ones) is able to predict the appearance of long-period IGWs from a high-frequency disturbance. This work makes it possible to explain generation of the secondary waves in the disturbances spectra. The results confirm the experimental fact that the main ionosphere response for all rocket launchings has a form of N wave both for AW and IGW.

[38] As for the data obtained by the transionosphere sounding of the upper atmosphere by signals of the satellite radio navigation system GPS, it is obvious from our results

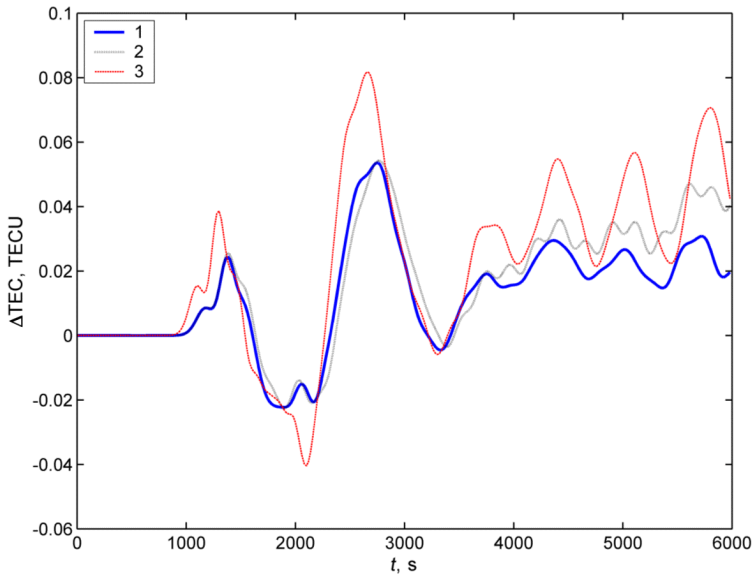

Figure 9. Time dependence of the vertical TEC disturbance in various models of the neutral atmosphere (see the text).

that the characteristic of these signals depends strongly on the receivers location, the satellite elevation angle, etc. Actually these disturbances are detected by the observers with the help of filtering the TEC time series within certain short intervals (3–5 min) in order to exclude the TEC variations due to the diurnal solar cycle [*Calais and Minster*, 1998]. However, our results show that the frequency range of these disturbances can be very wide. We see that the curve in Figure 8 qualitatively well describes the disturbances detected by *Calais and Minster* [1998]. The wave periods, delay time of the second packet relative the first packet, and horizontal phase velocities of the wave propagation almost coincide in our model and the experiment.

[39] The IGW predicted by us were registered in many experiments. Comparing Figure 1 to Figures 7 and 9 we see that our model predicts an appearance of the first wave with large amplitude and period and the secondary waves following after it with shorter periods and smaller amplitudes. Thus the developed numerical method well describes generation of all types of waves during rocket launchings.

[40] The disturbances amplitudes obtained are equal to 0.01–0.1 in the TECU units. It is confirmed in many observations [*Afraimovich et al.*, 2001; *Calais and Minster*, 1998]. However, as it has been noted above, our main goal was to study the common properties of the atmosphere and ionosphere disturbances generated by rocket flights at large distances.

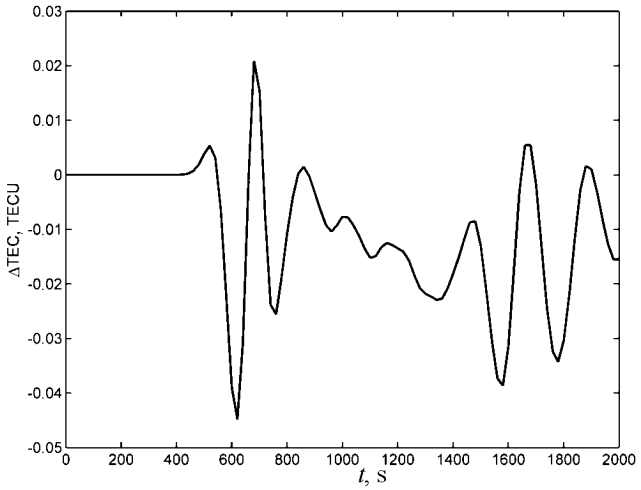

Figure 8. Time dependence of the slant TEC disturbance.

5. Conclusions

[41] A numerical model of the AGW propagation in the two-dimensional compressible atmosphere, taking into account the atmosphere stratification, zonal wind, dissipative effects, and nonlinearity was developed. The following results of this work may be important for the atmosphere physics: (1) development of a contemporary numerical method for the solution of problems of the intense atmosphere waves propagation to large distances; (2) simulation of the atmosphere disturbances caused by sources of various types including a supersonic rocket flight; and (3) investigation of time and spatial characteristics of the ionosphere disturbances generated by wave motions. The comparison of our results to the results of theoretical and experimental works of other authors shows that the developed method has high accuracy and effectiveness.

[42] It was found that the zonal wind and variation in the temperature profile depending on the season do not considerably influence the properties of the generated waves.

Analyzing the obtained results one can conclude that for precise interpretation of the observation data on the upper atmosphere state during rocket launchings one has to take into account the following parameters: (1) trajectory of the rocket flight; (2) parameters of SW generated by the rocket flight; (3) parameters of the Earth magnetic field over observation place; (4) method of registration (in the case of GPS measurements it is the orientation of the satellite-receiver ray, the receiver location, etc.); and (5) spatial distribution of the ionosphere electron concentration in the observation region during the disturbances registration.

[43] It follows from above that one should simulate ionosphere disturbances individually for each cases of rocket launching and calculate their manifestation for the given experimental method used by the observer. Moreover, the three-dimensional problem should be solved. However, all this is a subject of our future investigations.

[44] **Acknowledgment.** The paper was partly supported by the Russian Foundation for Basic Research, project 02-05-65350.

References

Adushkin, V. V., S. I. Kozlov, and A. V. Petrov, Eds., (2000), *Ecological Problems and Influence of the Rocket-Space Equipment on the Environment* (in Russian), 640 pp., Ankil, Moscow.

Afraimovich, E. L., E. A. Kosogorov, N. P. Perevalova, and A. V. Plotnikov (2001), The use of GPS arrays in detecting shock-acoustic waves generated during rocket launchings, *J. Atmos. Sol. Terr. Phys., 63,* 1941.

Andreeva, E. S. et al. (2001), Radiotomographic registration of the ionosphere disturbances from ground explosions, *Space Res.* (in Russian), *39*(1), 13.

Arendt, P. R. (1971), Ionospheric undulations following Apollo 4 launching, *Nature, 231,* 438.

Calais, E., and J. B. Minster (1998), GPS, earthquakes, the ionosphere, and the space shuttle, *Phys. Earth Planet. Inter., 105,* 167.

Durran, D. (1999), *Numerical Methods for Wave Equations in Geophysical Fluid Dynamics,* 465 pp., Springer-Verlag, New York.

Francis, S. H. (1975), Global propagation of atmospheric gravity waves: A review, *J. Atmos. Terr. Phys., 37,* 1011.

Gavrilov, N. M. (1985), Propagation of internal gravity waves in stratified atmosphere, *Phys. Atmos. Ocean* (in Russian), *21,* 921.

Jacobson, A. R., and R. C. Carlos (1994), Observations of acoustic-gravity waves in the thermosphere following space shuttle ascents, *J. Atmos. Terr. Phys., 56*(4), 525.

Karlov, V. D., S. I. Kozlov, and G. N. Tkachev (1980), Large-scale ionosphere disturbances generated at rocket flight with operating engine (a review), *Space Res.* (in Russian), *18*(2), 266.

Kunitsyn, V., and E. Tereshchenko (2003), *Ionospheric Tomography,* 272 pp., Springer-Verlag, New York.

Landau, L. D., and V. M. Lifshits (1988), *Fluid Dynamics* (in Russian), 733 pp., Nauka, Moscow.

Nagorsky, P. M. (1998), Modification of the ionosphere F region by a powerful pulse source of waves in the neutral gas, Dr. S. thesis, Tomsk State Univ., Tomsk.

Noble, S. T. (1990), A large-amplitude traveling ionospheric disturbance exited by the space shuttle during launch, *J. Geophys. Res., 95,* 19,037.

Oran, E. S., and J. P. Boris (1987), *Numerical Simulation of Reactive Flow,* Elsevier Sci., New York.

Rudenko, O. V., and S. I. Soluyan (1975), *Theoretical Fundamentals of Nonlinear Acoustics* (in Russian), 1423 pp., Nauka, Moscow.

Sedunov, Yu. S. (1991), *Atmosphere: Handbook* (in Russian), Gidrometeoizdat, St. Petersburg.

Tolstoy, I. et al. (1970), Long-period sound waves in the thermosphere from Apollo launches, *J. Geophys. Res., 75,* 5621.

Zhang, S. D., and F. Yi (2002), A numerical study of propagation characteristics of gravity wave packets propagating in a dissipative atmosphere, *J. Geophys. Res., 107*(D14), 4222.

R. R. Ahmadov and V. E. Kunitsyn, Faculty of Physics, Moscow State University, Moscow 119899, Russia.
(ravan@phys.msu.su)